

Article

Functionalized Bentonite Clay Composite with NiAl-Layered Double Hydroxide for the Effective Removal of Cd(II) from Contaminated Water

Muhammad Shafiq ¹, Abdulrahman Ali Alazba ^{1,2} and Muhammad Tahir Amin ^{1,3,*}¹ Alamoudi Water Research Chair, King Saud University, Riyadh 11451, Saudi Arabia² Agricultural Engineering Department, King Saud University, Riyadh 11451, Saudi Arabia³ Department of Environmental Sciences, COMSATS University Islamabad, Abbottabad Campus, Abbottabad 22060, Pakistan

* Correspondence: mtamin@ksu.edu.sa; Tel.: +966-11-467-3737; Fax: +966-11-467-3739

Abstract: In this study, the efficiency of functionalized bentonite (F-bentonite) and NiAl-layered double hydroxide (LDH), as well as their nanocomposites, was explored regarding the adsorption of cadmium ions (Cd^{2+}) in batch tests. Surface characterization using SEM, EDX, and FTIR analyses confirmed the successful loading of LDH (NiAl) onto the F-bentonite and the adsorption of Cd^{2+} onto the F-bentonite, LDH (NiAl), and LDH/F-bentonite composite adsorbent, suggesting ion exchange and surface precipitation as the main controlling mechanisms of the formation of adsorbent. An equilibrium contact period of 60 min was suggested, with the LDH/F-bentonite composite presenting the highest adsorption capacity and removal effectiveness as compared to the other adsorbents. The LDH/F-bentonite composite also presented the highest removal efficiency and maximum adsorption capacity at an optimum pH value of 7.0. A steady increase in the uptake capacity of Cd^{2+} was observed by increasing the dosage of the adsorbents, with the LDH/F-bentonite composite having the best adsorption capacity. The fitting of the pseudo second-order kinetic model to the adsorption data of Cd^{2+} suggested chemisorption on the adsorbents' surfaces as the controlling mechanism. The Langmuir isotherm with a near-perfect fitting revealed a monolayer adsorption, while physical adsorption of Cd^{2+} onto all the adsorbents is proposed using the D-R isotherm. Finally, both homogeneous and heterogeneous adsorption systems are proposed for all the adsorbents due to the satisfactory fitting of the Sips and R-P isotherm models.

Keywords: adsorption mechanism; composite adsorbents; kinetic and isotherm; optimum capacity; physical adsorption



Citation: Shafiq, M.; Alazba, A.A.; Amin, M.T. Functionalized Bentonite Clay Composite with NiAl-Layered Double Hydroxide for the Effective Removal of Cd(II) from Contaminated Water. *Sustainability* **2022**, *14*, 15462. <https://doi.org/10.3390/su142215462>

Academic Editor: Yi (Harvey) Huang

Received: 21 September 2022

Accepted: 15 November 2022

Published: 21 November 2022

Publisher's Note: MDPI stays neutral with regard to jurisdictional claims in published maps and institutional affiliations.



Copyright: © 2022 by the authors. Licensee MDPI, Basel, Switzerland. This article is an open access article distributed under the terms and conditions of the Creative Commons Attribution (CC BY) license (<https://creativecommons.org/licenses/by/4.0/>).

1. Introduction

Water is the most precious natural resource on earth and is essential for the survival of all living things. Every human being on earth has the right to drink clean and pure water [1]. Sadly, one out of every four people in the globe does not have access to safe drinking water, according to a report [2]. This is due to the fact that untreated effluents dumped into fresh water reservoirs are constantly polluting them with a variety of hazardous compounds such as dyes and heavy metals. Heavy metals are particularly important because they are poorly biodegradable and can remain in the environment for longer periods of time. The high levels of heavy metals in drinking water are primarily due to waste disposal from industries such as electroplating, mining, dyeing, paint manufacturing, fertilizers, and pharmaceuticals. Cadmium (Cd), lead (Pb), arsenic (As), copper (Cu), and mercury (Hg) are among the list of toxic heavy metals found in polluted water. The occurrence of certain heavy metals in drinking water beyond the allowed limit may pose substantial health concerns to humans [3]. It has been well-established that heavy metals are a major environmental problem with negative health consequences; thus, it is of critical importance

to act quickly in developing effective treatment technologies for the removal of heavy metals from heavy metal-rich industrial wastewater in order to reduce contaminants to acceptable levels [4].

Among various technologies used for wastewater treatment, adsorption technology is an ideal solution as it is inexpensive and adaptable to a wide range of pollutants found in diverse industrial effluents [5]. Adsorbents play an important role in the adsorption process. Adsorbent materials such as activated carbon [6], polymers [7], biomaterials [8], alumina [9], zeolite [10], and nanomaterials [11,12] have all been studied, and some have proven to be highly successful for heavy metal removal. However, there is still a need to develop new adsorbent materials with improved adsorption capacity to adsorb a variety of pollutants in contaminated water. In recent years, layered double hydroxide (LDH) has attracted the attention of researchers as a suitable choice for efficient adsorption processes due to its higher specific surface area; its various functional groups, especially hydroxyl (OH^-) ions; the reversibility of its structure, its strong exchange capacity, the ease of modifying layer spacing, and the flexibility of the metal composition [13–15]. Many studies have been undertaken to remove heavy metal efficiently from industrially complex polluted water by changing the metals and the $\text{M}^{+2}/\text{M}^{+3}$ metal ratios using LDH synthesis, depending on the application [16–19]. For instance, Moaty et al. [20] synthesized Co-Fe LDH and reported 95% removal of Cd ions from wastewater. Likewise, Ricardo Rojas [21] prepared Ca-Al LDH and reported higher adsorption capacities for copper, lead, and cadmium ions (Cd^{2+}). Dinari et al. [20] used poly vinyl alcohol to make an EDTA-ZnAl LDH nanocomposite and reported a Cd(II) adsorption capacity of 9.54 mg/g. Synthesizing LDH composites with a variety of well-known carbon-rich adsorbent materials or nanomaterials yielded excellent results [19,22–26].

In order to continue the quest for more effective and efficient combinations of LDH and adsorbent materials, this study aimed to synthesize functionalized bentonite (F-bentonite) with LDH of NiAl. Bentonite clay is an efficient adsorbent material because of its large specific surface area, its strong mechanical and chemical stability, its ability to be negatively charged and balanced with exchangeable cations, and its various surface and structural properties [27–29].

The objective of this research was to combine functionalized bentonite (F-bentonite) clay with NiAl-LDH to create a novel nanocomposite material that might preserve or even enhance the key characteristics of each phase while also generating new features through the interaction of these two materials. Therefore, this nanocomposite material was synthesized and tested for its efficacy in removing harmful Cd^{2+} by varying different parameters such as the shaking time, adsorbent dosage, pollutant concentration, and pH of the target solution. The findings of the study were intended to give insight into the use of LDH/F-bentonite as an effective adsorbent for heavy metal removal.

2. Materials/Chemicals and Methodology

2.1. Stock Solution Preparation

Cadmium nitrate ($\text{Cd}(\text{NO}_3)_2$) was obtained from Tianjin, Co., Ltd., (Tianjin, China), and a stock solution of 1 L was prepared by adding the required amount in double-distilled water. The stored stock solution was used to prepare the dilutions by using the double-distilled water so as to obtain the desired initial concentrations of Cd^{2+} , as per the requirement of each batch test. In addition, the analytical-grade solutions of sodium hydroxide and hydrochloric acid, each with 0.1 M concentration, were used for pH adjustment of the metal's solution, as per the requirement of each batch test.

2.2. Preparation of the Composite Adsorbents

Bentonite clay (bentonite) was used as one of the adsorbents in this study and was collected from the city of Riyadh in Saudi Arabia. The variable particle size of the collected bentonite was achieved by grounding and sieving. The functionalized bentonite clay was prepared by adding 1.5 g of the bentonite into an 80 mL mixture of NaOH (0.2 M) and

NaHCO_3 (0.05 M). The ultra-sonication of the mixture was performed for 30 min while complete dispersion of the bentonite clay in the solution was achieved by continuous stirring.

The LDH of NiAl with a ratio of 1:2 ($\text{Al}^{2+}/\text{Ni}^{3+}$) was prepared by mixing 0.3 M of aluminum nitrate nonahydrate ($\text{Al}(\text{NO}_3)_3 \cdot 9\text{H}_2\text{O}$) and 0.6 M of nickel (II) nitrate hexahydrate ($\text{Ni}(\text{NO}_3)_2 \cdot 6\text{H}_2\text{O}$) via the co-precipitation method. The continuous agitation of both solutions in deionized water was performed with a dropwise addition of the ammonia to maintain the solution's pH at 10.0 until the precipitate was performed within a time period of about 30 min.

The composite adsorbent of LDH and F-bentonite was prepared by dissolving appropriate concentrations of both salts in the required amount of double-distilled water. After achieving the complete dissolution of the salts with continuous stirring, the solution of the functionalized bentonite clay was added dropwise in this mixture. After 30 min of vigorous stirring, 1 M NaOH solution was added dropwise to obtain a solution pH of 10.0. The resulting precipitate was separated by centrifugation after maintaining the mixture at 60 °C for 3 h, and the pH neutrality was attained by extensive washing of the mixture using the deionized water. The final product was kept for 8 h in an oven at 80 °C and then placed in a desiccator for later use.

2.3. Characterization Techniques

The characterization of these adsorbents was performed using scanning electron microscopy (SEM) (HITACHI S-3000N, Kyoto, Japan), energy dispersive X-ray spectroscopy (EDX), and Fourier transform infrared (FTIR) spectroscopy. The SEM micrographs were obtained at magnifications of 250 \times , 500 \times , and 2000 \times before the treatment and the visibly porous nature of the adsorbents' surface were analyzed. The measurements were made at a working distance of 25 mm under an acceleration voltage of 5 kV, while a specified SEM steel stab holder was used to hold the dry powder samples. To avoid electrostatic charging of the samples, the steel stab holders were coated with a thin layer of platinum before being inserted into the SEM sample chamber to take the images under a high vacuum. EDX analysis was performed using the EDX detector, an optional accessory for the SEM. This detector allows the use of the generated X-rays as a signal to generate information about the chemical composition of the sample, including the elements present, their distribution, and their concentration. The attenuated total reflectance method was used for the FTIR spectroscopy using the Vertex-70 instrument (Bruker, Billerica, MA, USA) to determine the surface properties of the solid material with 16 sample scans at a spectral range of 600–4000 cm^{-1} and a resolution of 4 cm^{-1} . The aforementioned techniques provided an insight into the chemical composition as well as the morphology of these adsorbents before and after the adsorption of Cd^{2+} and were employed to examine the surface of the nanocomposite materials and to evaluate the mechanism involved in removing the target contaminant.

2.4. Measurement of the Adsorption Capacities and Removal Efficiencies

The sample solutions with the desired initial concentrations of Cd^{2+} were agitated in a temperature-controlled shaker (30 °C with 220 rpm, Wise Cube orbital), obtained from Daihan Scientific Co. Ltd., Wonju, Republic of Korea. Depending on the volume of the tested solution (50 or 100 mL) in conical flasks, the appropriate amount of each adsorbent was added depending on the initial concentration of Cd^{2+} so as to achieve the desired dose of the adsorbent as per the requirements of the specific batch test. After keeping them for a specified retention time, the sample solutions were filtered using a 0.45 μm Whatman™ filter, and a 5 mL sample was used further in flame atomic absorption spectrometry (FAAS, Thermo Scientific, ICE 3000 Series, Cambridge, UK). The light source (hollow-cathode lamp) specific to Cd^{2+} was adjusted after the flame optimized the inserted sample at a high temperature; its concentration was determined using the absorbance of the sample at its characteristic wavelength. FAAS was used to determine the residual metal concentration

(C_t , mg L^{-1}), while the adsorption capacity (q_t , mg g^{-1}) and the percentage removal of the Cd^{2+} were calculated using Equations (1) and (2), respectively.

$$\text{Adsorption capacity} = \left(\frac{C_0 - C_t}{m} \right) V \quad (1)$$

$$\text{Removal (\%)} = \left(\frac{C_0 - C_t}{C_0} \right) \times 100 \quad (2)$$

In the above equations, the solution volume and amount of adsorbent are expressed by V (L) and m (g), respectively, whereas the initial metal concentration is denoted by C_0 (mg L^{-1}).

2.5. Fitting of the Kinetic and Isotherm Models to the Adsorption Data

OriginPro 8.5 Software was used for the analysis and fitting of the original nonlinear expressions (Equations (3)–(8)) of the various kinetic models by plotting the uptake capacity (q_t , mg g^{-1}) of Cd^{2+} and the respective retention time (t , min), i.e., q_t vs. t . Equations (3) and (4) present the nonlinear and linearized form of the pseudo first-order kinetic model, respectively, while Equations (5) and (6) show the nonlinear and linearized form of the pseudo second-order kinetic model, respectively. Similarly, the nonlinear and linearized form of the Elovich model is presented in Equations (8) and (9), respectively. The calculated equilibrium adsorption capacities (q_e , mg g^{-1}) were then compared with the experimental values from the batch tests performed using 0.3 g of any adsorbent under a solution pH of 6.0 ± 0.2 .

$$q_t = q_e (1 - \exp(-k_1 t)) \quad (3)$$

$$\log(q_e - q_t) = \log q_e - \frac{k_1}{2.303} t \quad (4)$$

$$q_t = \frac{q_e^2 k_2 \cdot t}{q_e k_2 \cdot t + 1} \quad (5)$$

$$\frac{t}{q_t} = \frac{1}{k_2 q_e^2} + \frac{1}{q_e} t \quad (6)$$

$$q_t = K_{ip} t^{1/2} + C \quad (7)$$

$$q_t = \frac{1}{\beta} \ln(1 + \alpha \beta t) \quad (8)$$

$$q_t = \beta \ln(t) + \beta \ln(\alpha) \quad (9)$$

The above equations were further simplified to their respective linearized forms, and the slope and intercept values were used to compute the theoretical adsorption capacities. k_1 (min^{-1}) and k_2 ($\text{mg g}^{-1} \text{min}^{-1}$) represent the rate constants of the pseudo first-order (Equations (3) and (4)) and pseudo second-order (Equations (5) and (6)) kinetic models, respectively, whereas the rate constants of the intraparticle diffusion of the Weber and Morris (ID-WM, Equation (7)) and Elovich (Equations (8) and (9)) kinetic models are denoted by K_{ip} ($\text{mg g}^{-1} \text{min}^{1/2}$) and α ($\text{mg g}^{-1} \text{min}^{-1}$), respectively. C (mg g^{-1}) in Equation (7) denotes the boundary-layer thickness in the ID-WM kinetic model, whereas the β (g mg^{-1}) in Equations (8) and (9) represents the activation energy in the Elovich kinetic model.

Various two-parameter (Langmuir, Freundlich, Dubinin–Radushkevich, Halsey, Temkin, Harkins–Jura, Jovanovic, and Elovich) and three-parameter (Redlich–Peterson and Sips) isotherm models were applied to the adsorption data of Cd^{2+} on the used adsorbents to evaluate and compare the obtained theoretical values of the maximum adsorption capacities in each model with the experimental values. The adsorption performance was compared using the original nonlinear and derived linearized (wherever possible) isotherm models, as explained in Table 1.

Table 1. Nonlinear expressions of the two- and three-parameter isotherm models and explanation of parameters.

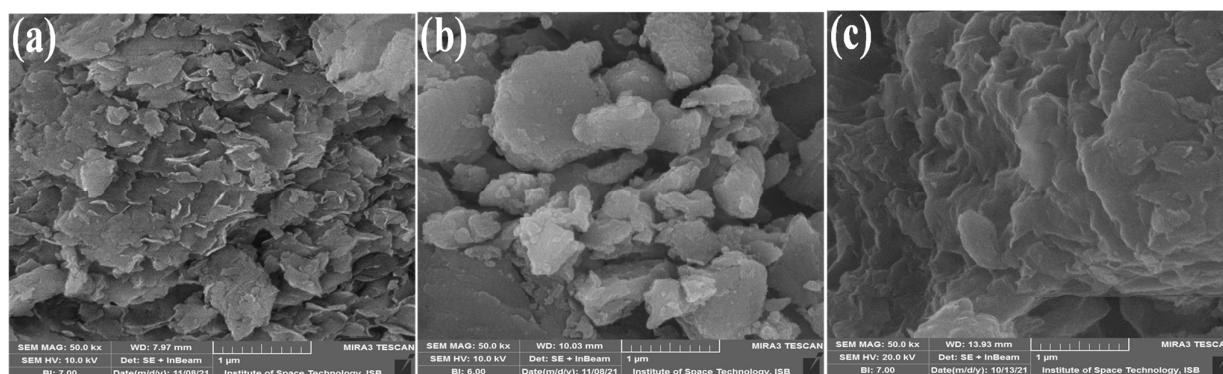
Isotherm Model	Mathematical Expression	Parameters
Langmuir	$q_e = \frac{q_m K_L C_e}{(1 + K_L C_e)}$	q_m , maximum sorption capacity, mg g^{-1} K_L , Langmuir constant, L mg^{-1}
Freundlich	$q_e = K_F C_e^{\frac{1}{n}}$	K_F , Freundlich constant, L g^{-1} n , dimensionless constant
Dubinin–Radushkevich	$q_e = q_m \exp(-K_{DR} \varepsilon^2)$ $\varepsilon = RT \ln(1 + 1/C_e)$ $E = 1/\sqrt{2K_{DR}}$	T , absolute temperature, Kelvin R , universal gas constant, $8.314 \text{ J mol}^{-1} \cdot \text{K}^{-1}$ E , mean free energy of adsorption, kJ mol^{-1}
Halsey	$q_e = \exp\left(\frac{\ln k_H - \ln C_e}{n_H}\right)$	n_H and k_H , Halsey constants
Temkin	$q_e = \frac{RT}{H_{ads}} \ln(K_T C_e)$	A_T , equilibrium binding constant, L g^{-1} b_T , heat of adsorption, kJ mol^{-1}
Harkins–Jura	$q_e = \left(\frac{A_{HJ}}{B_{HJ} - \log C_e}\right)^{\frac{1}{2}}$	A_{HJ} and B_{HJ} , H–J constants
Jovanovic	$q_e = q_m [1 - \exp(-k_j C_e)]$	k_j , Jovanovic constant
Elovich	$\frac{q_e}{q_m} = k_e C_e \exp\left(-\frac{q_e}{q_m}\right)$	k_e , Elovich constant α , L mg^{-1}
Redlich–Peterson	$q_e = \frac{K_{RP} C_e}{1 + \alpha C_e^\beta}$	β (0–1), dimensionless K_{RP} , R–P constant, L g^{-1}
Sips	$q_e = \frac{q_m K_S C_e^n}{1 + K_S C_e^n}$	n , degree of heterogeneity, dimensionless K_S , energy of adsorption, L g^{-1}

3. Results and Discussion

3.1. Characteristics of the Adsorbents and Adsorption Mechanism

3.1.1. Scanning Electron Microscopy Analysis

SEM techniques were used to study the surface morphology, texture, and particle size/distribution of the samples. The F-bentonite surface structure, the LDH (NiAl), and the LDH/F-bentonite composites were analyzed using SEM and are shown in Figure 1a–c. The F-bentonite (Figure 1a) sample looked to be exceedingly compact in the SEM images, with layered and flaked morphology. The F-bentonite particles were crystalline with regular-shaped morphology. Figure 1b shows that the surface morphology of the LDH (NiAl) displayed compact aggregates of irregular shapes. Figure 1c shows the surface structure of the LDH/F-bentonite composite materials. It is obvious from the SEM images that the surface morphology of the composite material was changed more significantly than that of the F-bentonite and LDH (NiAl). The LDH/F-bentonite composites were composed of a rigid irregular sheet-like structure. This could be due to the LDH particles having filled up the internal and external spaces of the bentonite, thereby generating a layered structure. The compact and layered structure could be due to the stronger electrostatic interactions between the bentonite (negatively charged) and LDHs (positively charged).

**Figure 1.** SEM images of F-bentonite (a), LDH (NiAl) (b), and LDH/F-bentonite composite (c).

3.1.2. Energy Dispersive X-ray Analysis

EDX analyses were used to validate the successful formation of composites and Cd^{2+} adsorption onto the surface or interlayer of the adsorbents tested, as depicted in Figure 2. The EDX spectra of the F-bentonite Figure 2a,d before and after Cd^{2+} adsorption revealed that the F-bentonite was made up of O, Na, Mg, Al, Si, Ca, and Fe, with weight percentages of 56.14%, 2.12%, 1.63%, 6.93%, 24.70%, 1.68%, and 6.80%, respectively. These materials demonstrated a rough surface. Similarly, the EDX spectrum of the F-bentonite after adsorption of Cd^{2+} exhibited certain changes in the elemental weight percentages and the addition of 1.21% Cd^{2+} as evidence of adsorption on the surface of the F-bentonite. The EDX spectra for LDH (NiAl) (Figure 2b,e) before and after adsorption of Cd^{2+} indicated that the LDH (NiAl) was composed of C (18.23%), O (51.19%), Na (0.95%), Al (4.89%), and Ni (24.74%). Furthermore, the spectrum after adsorption (Figure 2e) showed a change in the elemental weight percentage and indicated the addition of 0.94% Cd^{2+} , proving that adsorption of Cd^{2+} occurred in the LDH (NiAl). Additionally, the EDX spectra of the LDH/F-bentonite composites (Figure 2c,f) before and after adsorption of Cd^{2+} revealed that the LDH/F-bentonite composite was made up of C (11.16%), O (45.33%), Na (1.12%), Mg (0.75%), Al (5.61%), Si (9.26%), Ca (1.42%), Fe (3.45%), and Ni (21.90%). Moreover, the spectrum after adsorption (Figure 2f) revealed changes in the elemental weight percentage and demonstrated the addition of 2.75% Cd^{2+} , proving that adsorption of Cd^{2+} occurred in the LDH/F-bentonite composite.

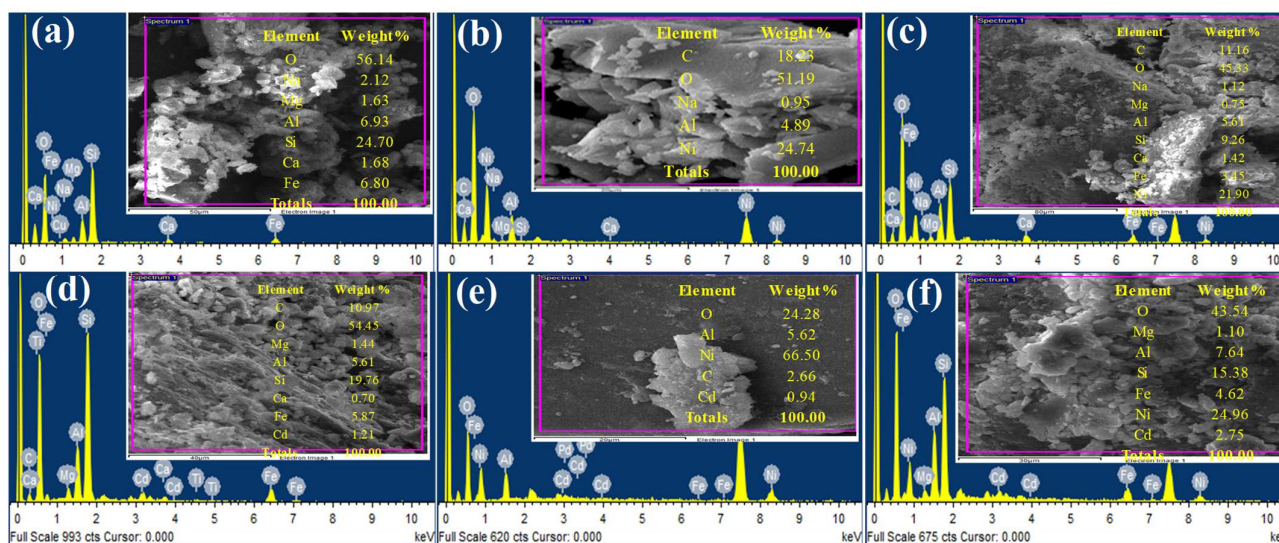


Figure 2. EDX micrograph showing before and after the adsorption of Cd^{2+} , F-bentonite (a,d), LDH (NiAl) (b,e), and LDH/F-bentonite composite (c,f).

3.1.3. Fourier Transform Infrared Analysis

The FTIR technique was employed to detect changes in the material composition before and after the adsorption of Cd^{2+} by observing alterations in the characteristic pattern of the absorption bands. The FTIR spectrograms of the F-bentonite, LDH (NiAl), and LDH/F-bentonite composites before and after Cd^{2+} adsorption are presented in Figure 3a,b. The FTIR plots of all the investigated materials before and after adsorption showed some slight changes, indicating that the functional groups changed after Cd^{2+} adsorption. The broad band at approximately $3200\text{--}3600\text{ cm}^{-1}$ in the pre-adsorption spectra (Figure 3a) is attributed to the stretching vibration of the surface hydroxyl groups bonded to the physically adsorbed water [30]. This band broadens in the post-adsorption spectrum (Figure 3b), indicating that the surface hydroxyl groups were engaged in the adsorption process [31]. A very-low-intensity peak at 1640 cm^{-1} in the pre-adsorption spectra of all the investigated materials (Figure 3a) belonged to OH frequencies of the adsorbed interlayer water molecules [32]. This band was shifted to 1626 cm^{-1} in the post-adsorption

spectra (Figure 3b). Additionally, a very prominent band appeared at 1367 cm^{-1} in the pre-adsorption (Figure 3a) spectra of the LDH (NiAl) and LDH/F-bentonite, which belonged to the N–O bending vibration of NO_3^- ions [33,34]. In addition, this band was shifted to 1358 cm^{-1} in the pre-adsorption (Figure 3b) spectra of the LDH (NiAl) and LDH/F-bentonite. This band was missing in the pre- and post-adsorption spectra of the F-bentonite. The characteristic absorption band at 1012 cm^{-1} was seen in the F-bentonite's pre-adsorption spectra (Figure 3a), which was shifted to 1005 cm^{-1} in the post-adsorption spectra (Figure 3b), belonging to the Si–O bending vibration. The higher intensity of the Si–O band in the F-bentonite (before and after adsorption) was due to the presence of silica tetrahedral sheets in the bentonite clay structure. Moreover, the LDH/F-bentonite also had this absorption band, indicating that the LDHs (NiAl) were loaded on the F-bentonite successfully [35,36]. The bands identified within the $500\text{--}1000\text{ cm}^{-1}$ region under the low frequency of the spectrum belonged to the vibration modes of M–O and M–OH [35,37]. The bands at 770 , 731 , and 690 cm^{-1} in the pre-adsorption spectra (Figure 3a) belonged to traces of carbonate ions present in the interlayer. Small shifts in these bands observed in the spectrum after adsorption (Figure 3b).

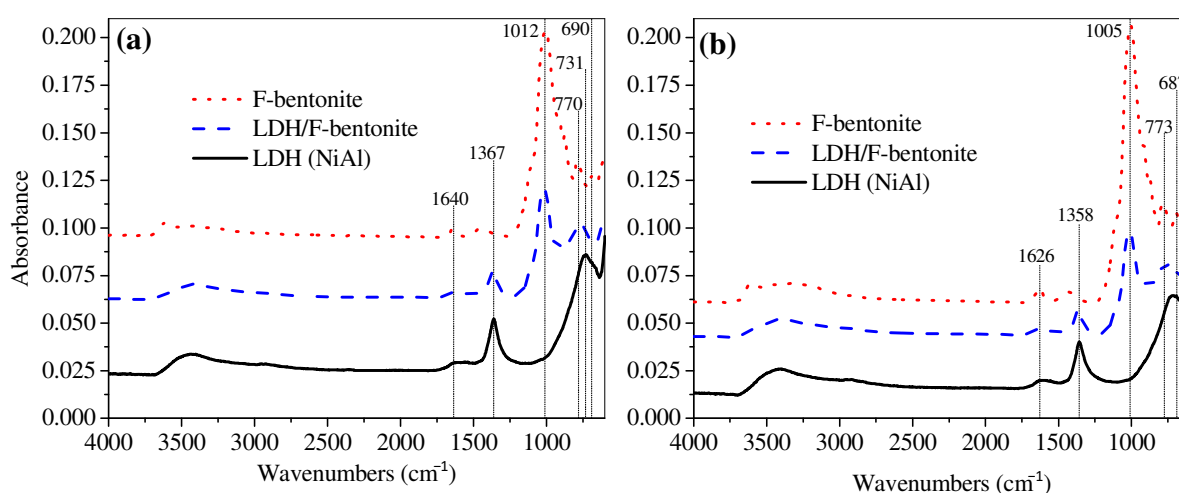


Figure 3. FTIR spectrograms of F-bentonite, LDH (NiAl), and LDH/F-bentonite composite before (a) and after adsorption of Cd^{2+} (b).

3.2. Effects of the Retention Time, Solution pH, and Initial Concentrations of the Adsorbent and Adsorbate

The equilibrium contact time was estimated due to its importance for any batch system to be able to efficiently utilize the adsorbent and to optimize the performance of the studied adsorption process. The changes in the adsorption capacity and removal efficiencies of the studied adsorbent for Cd^{2+} with the changes in retention time (1 min to 5 h) are shown in Figure 4. The evaluation of the adsorption system was performed by selecting 5 and 20 mg L^{-1} of Cd^{2+} , employing 0.3 g of each adsorbent while keeping the pH of the solution at 6.0. The lowest performance with respect to adsorption capacity and removal efficiency was seen for the LDH (NiAl) as compared with the other adsorbents, while the composite adsorbent (LDH/F-bentonite) presented the highest adsorption capacities and removal efficiencies at the respective retention times. A steady uptake of Cd^{2+} was seen up to a retention time of 60 min after observing a rapid removal within 5 min because of the presence of free active sites upon immediate contact (especially for 5 mg L^{-1} of Cd^{2+} , Figure 4a) using all the adsorbent with little changes afterwards until 120 min of contact time (except for the LDH/F-bentonite adsorbent), as shown in Figure 4. As a result, a retention time of 60 min was taken as the equilibrium contact time for the current adsorption system, with little to no changes in the uptake or removal of the studied metal ion, even up to a retention time of 5 h, as shown in Figure 4. This is because the free active sites on the surface of the adsorbent were already saturated. The highest uptake of nearly 60 mg g^{-1}

(with a removal efficiency of 59%) for 20 mg L^{-1} of Cd^{2+} was observed when using the composite adsorbent of LDH/F-bentonite, which also resulted in a maximum removal efficiency of nearly 90% (with a corresponding adsorption capacity of 22.5 mg g^{-1}) for 5 mg L^{-1} of Cd^{2+} .

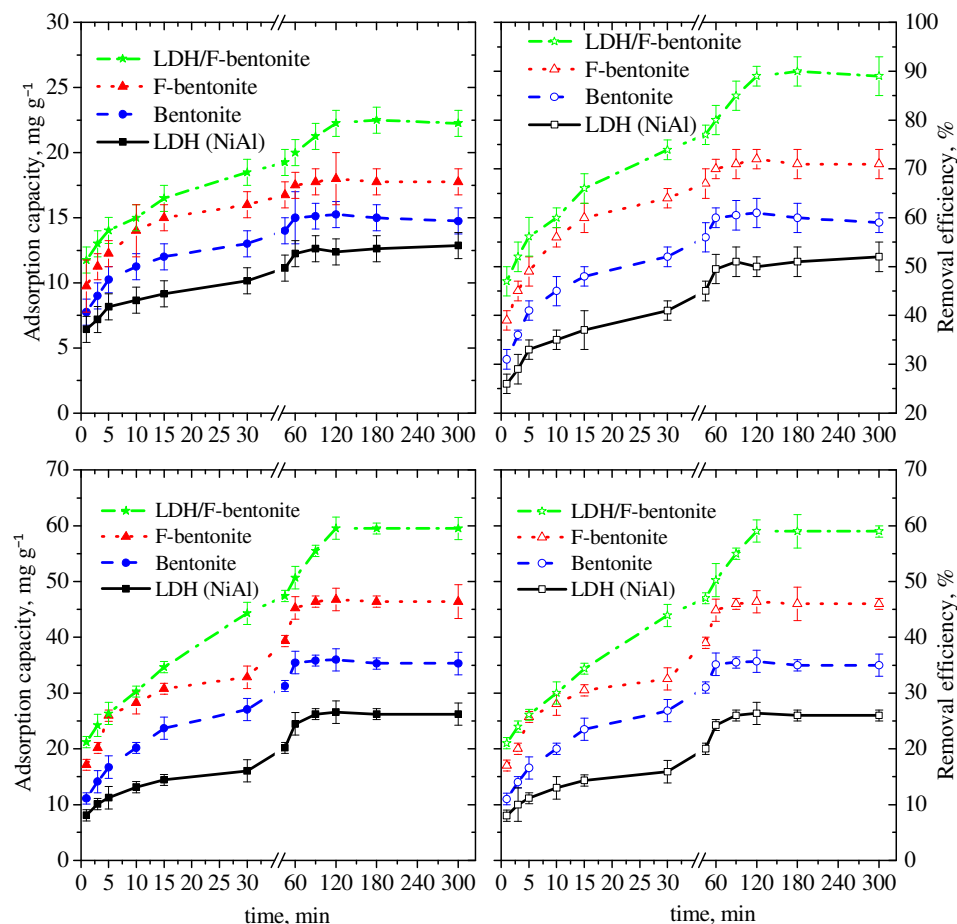


Figure 4. Effect of the contact time on the adsorption capacities and removal efficiencies of the studied adsorbents at 5 and 20 mg L^{-1} of Cd^{2+} (solution pH, 6 ± 0.2 ; adsorbent dose, 0.3 g ; and initial Cd^{2+} concentration, 5 and 20 mg L^{-1}).

The changes in the uptake and removal efficiencies of Cd^{2+} with respect to varying values (3–9) of the solution's pH are presented in Figure 5a. A constant dose of each adsorbent (0.3 g) was selected with 20 mg L^{-1} of Cd^{2+} at an already-estimated equilibrium contact period of 60 min . The presence of a high amount of H^+ at low pH values (2–3) resulted in very high competition between the positively charged ions, and hence a poor adsorption performance was observed. With the increase in solution pH, a smaller amount of H^+ resulted in an increased attachment of the divalent Cd^{2+} attaching to the adsorbent's surface [38–40]. An optimum performance at a near-neutral pH value of 7.0 was observed for all the adsorbents with little or insignificant changes with further increases in solution pH, as shown in Figure 5a. The highest removal efficiency of nearly 58% with a corresponding maximum adsorption capacity of 58.5 mg g^{-1} was observed for the composite adsorbent of LDH/F-bentonite, while the LDH (NiAl) adsorbent showed the poorest performance as compared with the other adsorbents (Figure 5a). Conclusively, a pH value of 7.0 ± 0.2 can be considered as an optimum value for the best performance of the studied adsorption system.

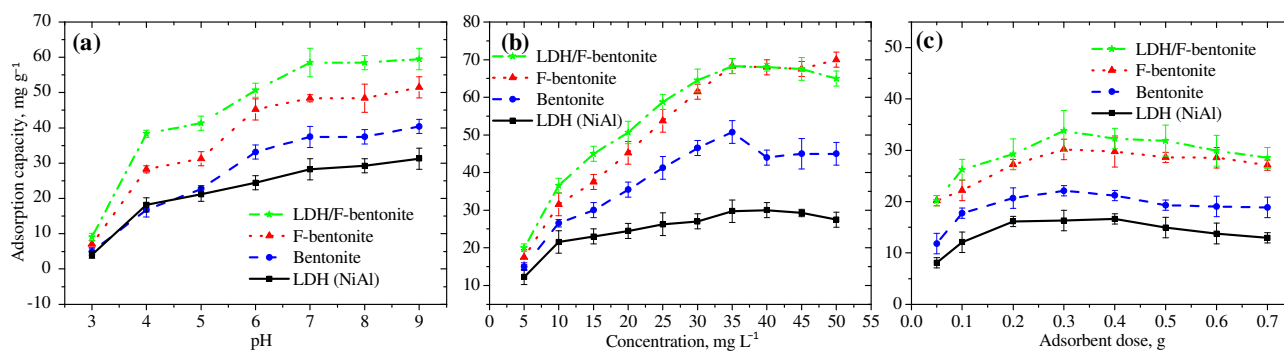


Figure 5. Effects of the solution pH (a), adsorbent dose (b), and initial Cd²⁺ concentration (c) on the adsorption capacities of Cd²⁺ by bentonite, F-bentonite, LDH (NiAl), and the composite (LDH/F-bentonite) (equilibrium contact time, 60 min; solution pH, 6 ± 0.2; initial Cd²⁺ concentration, 20 mg L⁻¹; and adsorbent dose, 0.3 g).

The initial Cd²⁺ concentration was calibrated for the best possible performance of the adsorption system by selecting its suitable range (5–50 mg L⁻¹), and its effects on both the adsorption capacities and removal efficiencies are shown in Figure 5b. A fixed (0.3 g) amount of each adsorbent with a solution pH of 6.0 was used, and the samples were retained for 60 min, which was considered to be the equilibrium contact time. A concentration of 35 mg L⁻¹ of Cd²⁺ was determined to be the ideal value for the optimal adsorption system performance of all the adsorbents, as shown in Figure 5b. Both the F-bentonite and LDH/F-bentonite adsorbents yielded the maximum adsorption capacity of about 68 mg g⁻¹ because of the presence of a powerful driving force causing the high Cd²⁺ (35 mg L⁻¹) to attach to the adsorbent's surface [41,42]. The linear increasing trend of the adsorption capacity with an increasing initial Cd²⁺ concentration reversed with insignificant decrease as the preliminary concentration increased from 35 to 50 mg L⁻¹. The removal efficacy, however, showed a decreasing trend with an increasing initial Cd²⁺ concentration due to the limited number of active sites of a set dosage (0.3 g) of the adsorbent attracting an increasing amount of Cd²⁺. The removal efficiency was estimated to be 35%, corresponding to the optimum Cd²⁺ value with the highest adsorption capacity for both the F-bentonite and LDH/F-bentonite adsorbents.

The effects of the changing dosage of each adsorbent within a suitable range (0.05–0.7 g) on the uptake and removal of Cd²⁺ at a fixed concentration of 20 mg L⁻¹ are shown in Figure 5c. The samples were agitated for a 60 min equilibrium contact period during which their pH was maintained at 6.0. A steady increase in the uptake capacity of Cd²⁺ was observed by increasing the dosage of the adsorbents from 0.05 g to up to 0.3 g due to the increasing active sites on the surface of the adsorbents at a predetermined concentration of Cd²⁺ (20 mg L⁻¹). The observed maximum values of the adsorption capacities were about 34 and 17 mg g⁻¹ (Figure 5c) for the LDH/F-bentonite composite adsorbent and bentonite, respectively. The removal efficiency followed a steady increasing trend simply due to the greater availability of the exchangeable adsorption sites with increases in the adsorbent dosage, reaching about 99% efficiency for the LDH/F-bentonite composite at the highest tested dosage of 0.7 g.

3.3. Application of Kinetic Models to the Adsorption Data

The adsorption data were explained using the pseudo first-order, pseudo second-order, ID-WM, and the Elovich kinetic models at various initial Cd²⁺ concentrations (5, 10, 15 and 20 mg L⁻¹). Table 2 shows the results of a quick comparison that was performed using only 5 mg L⁻¹ of Cd²⁺, using both the original nonlinear and derived linearized kinetic models to compare the experimental and calculated adsorption capacities.

Table 2. Estimated values of the parameters using nonlinear and derived linearized kinetic models at 5 mg L⁻¹ of Cd²⁺ onto 0.3 g of adsorbent at pH = 6 ± 0.2.

Kinetic Model	Parameter	Nonlinear				Linearized			
		Bentonite	F-Bentonite	LDH (NiAl)	LDH/F-Bentonite	Bentonite	F-Bentonite	LDH (NiAl)	LDH/F-Bentonite
Pseudo 1st-order	$q_{e \text{ exp}}$ (mg g ⁻¹)	15.00	17.50	12.25	20.00	15.00	17.50	12.25	20.00
	$q_{e \text{ cal}}$ (mg g ⁻¹)	13.9	16.57	11.34	16.63	3.55	2.90	2.92	3.31
	k_1 (min ⁻¹)	0.38	0.45	0.35	0.4	0.009	0.006	0.006	0.006
	R^2	0.56	0.55	0.45	0.39	0.75	0.38	0.49	0.4
Pseudo 2nd-order	$q_{e \text{ cal}}$ (mg g ⁻¹)	14.59	17.32	11.99	20.73	14.99	17.95	13.00	22.68
	k_2 (g mg ⁻¹ min ⁻¹)	0.0426	0.0431	0.0443	0.0292	0.0355	0.0271	0.0167	0.0096
	h (mg g ⁻¹ min ⁻¹)	9.07	12.93	6.37	12.55	7.99	8.73	2.82	4.96
	R^2	0.83	0.84	0.74	0.71	0.9994	0.9998	0.9994	0.9992
ID-WM	K_{ip} (mg g ⁻¹ min ^{1/2})	0.42	0.47	0.41	0.7	0.4289	0.51	0.41	0.70
	C (mg g ⁻¹)	9.73	12.06	7.45	13.21	9.7275	11.30	7.45	13.21
	R^2	0.66	0.65	0.79	0.82	0.69	0.75	0.81	0.84
Elovich	α (mg g ⁻¹ min ⁻¹)	355.17	570.01	136.09	329.82	245.95	907.48	106.16	153.56
	β (g mg ⁻¹)	0.69	1.59	0.77	0.46	1.45	0.63	1.30	2.17
	R^2	0.93	0.94	0.96	0.97	0.94	0.94	0.96	0.97

Neither the nonlinear nor the linearized fitting of the pseudo first-order kinetic model produced reasonable results, as reflected from the calculated R^2 values lying mostly within the average range of 0.40–0.55 for both 5 (Table 2) and 20 mg L⁻¹ of Cd²⁺, suggesting a poor fit. Moreover, significantly low adsorption capacities were calculated in the linearized approach as compared to the experimental values, whereas a close match between both the calculated and experimental adsorption capacities was observed for the nonlinear pseudo first-order kinetic model. A very close match between the predicted and experimental adsorption capacities is another indication of how perfectly both the nonlinear and linearized pseudo second-order kinetic model fitted, as presented in Table 2. The lowest-rate constant was observed for the composite adsorbent of LDH/F-bentonite as compared with the other adsorbents using either the nonlinear or the derived linearized fitting of the pseudo second-order kinetic model (Table 2). The activation energy of the LDH/F-bentonite composite adsorbent in the nonlinear Elovich kinetic model was the lowest as compared with the other adsorbents, whereas the highest value was observed for the same adsorbent in the linearized fitting (β in Table 2). Both the nonlinear and the linearized fitting of the ID-WM kinetic model yielded average R^2 values (0.65–0.84, Table 2) with the highest values for the model's constant and boundary-layer thickness of the LDH/F-bentonite composite as compared with the other adsorbents used in this study. Due to their good-fitting, both the nonlinear fitting and the derived linearized models of the pseudo second-order and the Elovich kinetic models applied to the experimental data of batch tests at 5 mg L⁻¹ of Cd²⁺ employing all the adsorbents are shown in Figure 6.

A precise linearized fit of the pseudo second-order kinetic model can be seen in Figure 6b with a coefficient of determination (R^2) close to unity (1.0). The same can also be seen for 5 mg L⁻¹ of Cd²⁺ with very high R^2 values, as presented in Table 2, signifying chemisorption as the controlling mechanism for the adsorption of Cd²⁺ onto the adsorbents' surfaces [43–45]. Similarly, both the nonlinear and the linearized fitting of the Elovich kinetic model yielded high R^2 values (0.93–0.97, Figure 6c,d) for 20 mg L⁻¹ of Cd²⁺, and the same can be observed for 5 mg L⁻¹ of Cd²⁺ (Table 2). The nonlinear fitting of the pseudo second-order kinetic model yielded only reasonable results with R^2 values mostly lying in the range of 0.71–0.84 for both concentrations of Cd²⁺ (Figure 6a and Table 2).

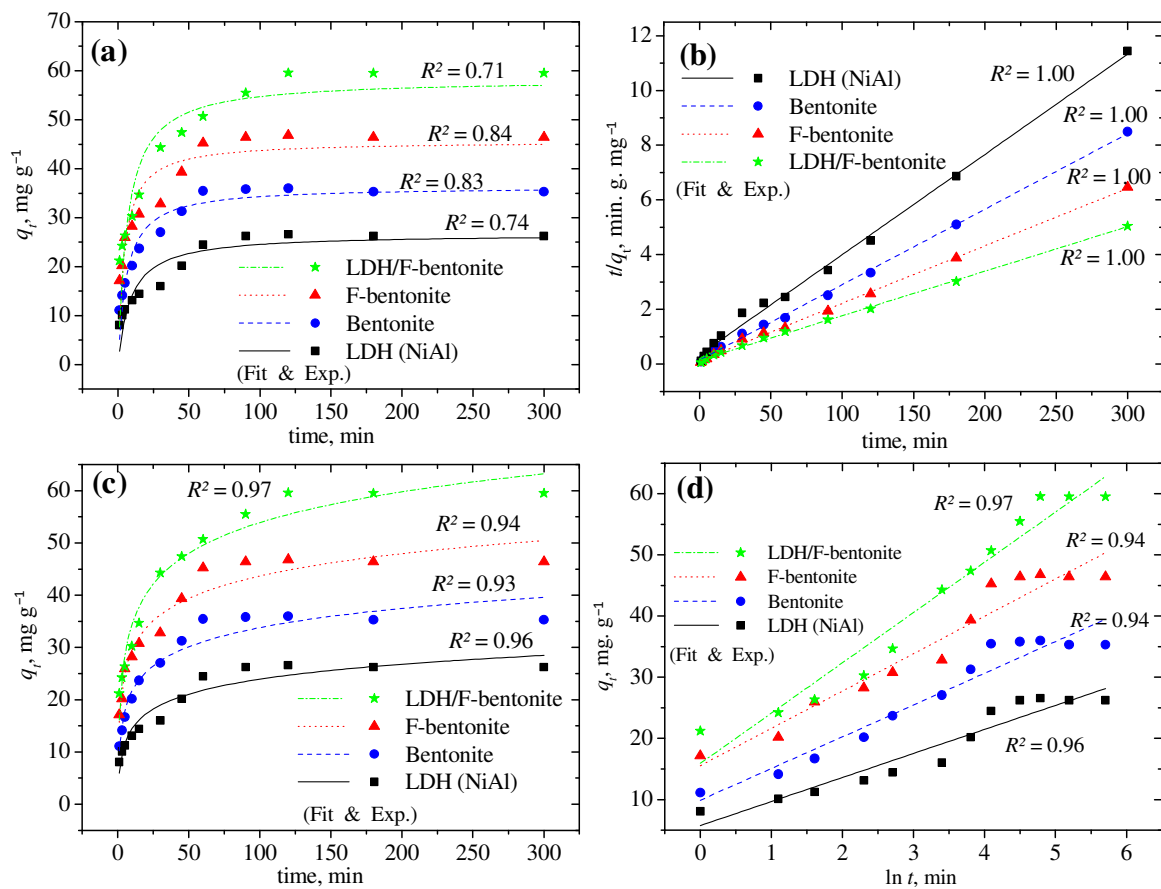


Figure 6. Nonlinear and derived linearized fitting of the pseudo-second-order (a,b) and the Elovich (c,d) kinetic models at 5 mg L^{-1} of Cd^{2+} .

3.4. Application of Different Isotherm Models to the Adsorption Data

The maximum adsorption capacities and the related parameters were calculated using the slope and intercept values when using the derived linearized approaches in each model. For the original nonlinear approaches, residual metal concentrations of Cd^{2+} at $5\text{--}50 \text{ mg L}^{-1}$ were used against the respective experimental adsorption capacities using 0.3 g of each adsorbent, while suspensions at a pH of 6.0 ± 0.2 were agitated for an equilibrium contact time of 60 min . Figure 7 presents the nonlinear and the derived linearized fittings of the Langmuir and Freundlich isotherms, with these being the most commonly used models. Both the nonlinear and linearized approaches of the Langmuir isotherm showed a near-perfect fitting to the adsorption of Cd^{2+} with very high R^2 values ($0.91\text{--}0.99$, Figure 7a,b) using all the adsorbents, signifying a monolayer adsorption system. The fitting of the Freundlich model is also supported based on the average R^2 value of 0.9 (Figure 7c,d) for all the adsorbents. For both models, the linearized approaches yielded better fittings as compared with the nonlinear approaches, as predicted when comparing the R^2 values.

The ability of both models to predict the adsorption data is further reflected in the permissible values of the separation factor [$R_L = (1 + K_L C_0)^{-1}$] and adsorption intensities ($n > 1$, Table 3) [46] in the Langmuir and the Freundlich isotherms, respectively. For both models, however, the maximum adsorption capacities were overestimated (with few exceptions) as compared to the experimental values, especially for the F-bentonite and the LDH/F-bentonite composite adsorbent. Moreover, the composite adsorbent of LDH-F/bentonite showed the highest K_F as compared with the other adsorbents in the Freundlich model. Moreover, the composite adsorbent showed a strong affinity between its surface and divalent Cd^{2+} , as predicted by the Langmuir isotherm due to it having the

highest K_L values as compared with the other adsorbents (Table 3) using both the nonlinear and linearized approaches.

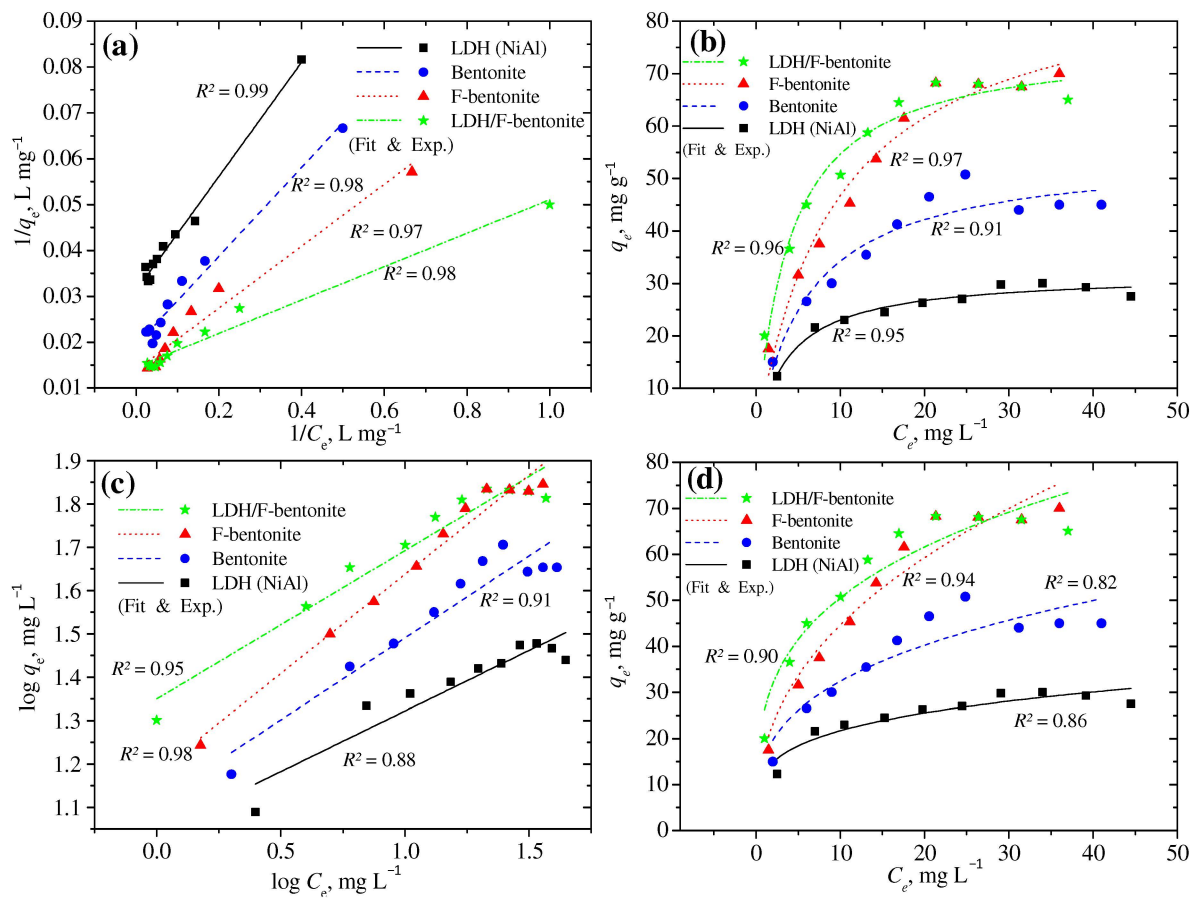


Figure 7. Nonlinear and derived linearized fittings of the Langmuir (a,b) and the Freundlich (c,d) isotherm models.

For the D–R and the Halsey and Temkin isotherms, the derived linearized models presented a better fitting than the nonlinear approach for all the adsorbents, based on the calculated R^2 values (Table 3), while the opposite trend was seen for the H–J and the Jovanovic isotherms. The D–R isotherm also predicted a physical adsorption of Cd^{2+} onto all the adsorbents due to the estimated E values ($<8 \text{ kJ mol}^{-1}$, Table 3) [47–49]. The calculated adsorption capacities in the D–R isotherm were slightly lower than the experimental values especially for those of the bentonite and the LDH-F/bentonite composite adsorbent when using the linearized approach. With respect to the calculated R^2 values, the Jovanovic isotherm proved to have a better fit to the adsorption data when using the nonlinear approach as compared with the other two-parameter models, with the exception of the Langmuir isotherm. The LDH-F/bentonite composite adsorbent showed lower heat of adsorption than that of the bentonite or LDH (NiAl) adsorbents, as predicted in the Temkin isotherm (Table 3). The calculated R^2 values within a suitable range of 0.88–0.96 in the Temkin model also suggested heterogeneous adsorption of Cd^{2+} with uniform dispersal of binding energies on the surface of the adsorbent [50]. Both of the three-parameter isotherms (Redlich–Peterson and Sips) fitted the adsorption data reasonably well, with an average high R^2 value of 0.96 (Table 3), indicating both homogeneous and heterogeneous adsorption of Cd^{2+} onto the adsorbent surfaces [51–54]. A relatively high heat of adsorption with a low degree of heterogeneity for the LDH/F-bentonite composite (0.28 L g^{-1} and 0.83 , respectively, Table 3) was estimate in the Sips model in comparison to the other adsorbents.

Table 3. Values of the parameters in the nonlinear and derived linearized fittings of the isotherm models (solution pH, 6 ± 0.2 ; contact time, 60 min; and adsorbent dose, 0.3 g).

Isotherm	Parameter	Nonlinear					Linearized			
Langmuir	q_m , mg g ⁻¹	54.92	90.32	31.82	76.07	51.81	71.94	32.05	68.49	
	K_L , L mg ⁻¹	0.17	0.11	0.26	0.26	0.20	0.21	0.25	0.40	
	R_L	0.144	0.206	0.099	0.099	0.125	0.122	0.102	0.067	
	R^2	0.91	0.97	0.95	0.96	0.98	0.97	0.99	0.98	
Freundlich	q_m , mg g ⁻¹	47.60	74.79	29.60	73.47	57.77	85.58	31.34	80.84	
	K_F , (mg/g)(L/mg) ^{1/n}	15.81	17.41	12.61	26.20	15.05	16.81	11.62	23.92	
	$1/n$	0.310	0.410	0.240	0.290	0.378	0.458	0.279	0.343	
	R^2	0.82	0.94	0.86	0.9	0.91	0.98	0.88	0.95	
D-R	q_m , mg g ⁻¹	45.82	68.29	27.54	66.27	41.42	56.45	27.26	58.84	
	K_{DR} , (mol kJ ⁻¹) ²	3.8×10^{-6}	5.0×10^{-6}	1.3×10^{-6}	2.2×10^{-6}	1.0×10^{-6}	8.0×10^{-7}	1.0×10^{-6}	4.0×10^{-7}	
	E , kJ mol ⁻¹	0.36	0.32	0.62	0.48	0.71	0.79	0.71	1.12	
	R^2	0.69	0.81	0.84	0.76	0.80	0.73	0.91	0.80	
Halsey	$q_{e\text{ cal}}$, mg g ⁻¹	46.35	66.59	29.24	67.53	54.66	105.76	27.82	93.42	
	n_H	-3.21	-2.45	-4.25	-3.51	-2.64	-2.18	-3.58	-2.92	
	K_H	0.000	0.001	0.000	0.000	0.356	0.447	0.225	0.391	
	R^2	0.82	0.94	0.86	0.90	0.91	0.98	0.88	0.95	
Temkin	K_T , L mg ⁻¹	1.96	1.35	4.70	3.95	1.96	1.35	4.70	3.95	
	H_{ads} , kJ mol ⁻¹	0.089	0.054	0.18	0.07	224.31	136.93	441.39	176.14	
	R^2	0.88	0.95	0.91	0.95	0.89	0.95	0.92	0.96	
	A_{HJ} , mg g ⁻¹	111.41	115.98	93.85	172.4	370.3704	500	270.27	769.231	
H-J	B_{HJ}	2.72	2.31	3.16	2.73	1.56	1.45	1.78	1.46	
	R^2	0.75	0.87	0.80	0.83	0.79	0.82	0.75	0.79	
	q_m , mg g ⁻¹	46.63	71.75	28.17	66.56	23.18	27.06	17.63	33.83	
	k_j , L g ⁻¹	-0.13	-0.11	-0.19	-0.19	-0.022	-0.034	-0.014	-0.025	
Elovich	R^2	0.91	0.96	0.91	0.94	0.61	0.73	0.58	0.60	
	q_m , mg g ⁻¹					21.41	36.10	8.92	23.15	
	k_e , L g ⁻¹					1.13	1.08	1.43	1.18	
	R^2					0.77	0.91	0.84	0.91	
R-P	K_{RP} , L g ⁻¹	6.09	10.15	7.96	21.54					
	α , L mg ⁻¹	0.0432	0.13	0.24	0.32					
	β	1.25	0.97	1.01	0.97					
	R^2	0.91	0.96	0.95	0.96					
Sips	q_m , mg g ⁻¹	53.99	102.36	31.51	81.94					
	K_S , L g ⁻¹	0.16	0.12	0.25	0.28					
	n_S	1.04	0.84	1.03	0.83					
	R^2	0.89	0.96	0.95	0.96					

Summarizing the fitting of the kinetic models, a perfect linearized fitting of the pseudo second-order kinetic model with an R^2 value close to unity 1.0 suggested chemisorption as the controlling mechanism for the adsorption of Cd²⁺ onto the adsorbents' surfaces. The nonlinear Elovich kinetic model yielded the lowest activation energy of the LDH/F-bentonite composite, whereas the highest value was observed in case of the linearized fitting of the same model. Both the nonlinear and the linearized fitting of the Langmuir isotherm with very high R^2 values (0.91–0.99) reflected a near-perfect fitting to the adsorption of Cd²⁺ using all the adsorbents, signifying a monolayer adsorption system. The physical adsorption of Cd²⁺ onto all the adsorbents is proposed due to the estimated E values (<8 kJ mol⁻¹) in the D-R isotherm. The suitable fitting of the Temkin model also suggested heterogeneous adsorption of Cd²⁺ onto the surface of the LDH-F/bentonite composite adsorbent, reflecting a lower heat of adsorption than that of the bentonite or LDH (NiAl) adsorbents. The Jovanovic isotherm showed a better fit of the adsorption as compared with the other two-parameter models, with the exception of the Langmuir isotherm, based on the calculated R^2 values. Finally, both homogeneous and heterogeneous adsorption of Cd²⁺ onto the surface of adsorbents is proposed due to the satisfactory fitting of the three-parameter models (Redlich–Peterson and Sips) with a relatively high heat of adsorption and a low degree of heterogeneity for the LDH/F-bentonite composite adsorbent in comparison with the other adsorbents, as estimated in Sips model.

4. Conclusions

Nanocomposites of functionalized bentonite clay and LDH of NiAl (LDH/F-bentonite) were tested for their efficacy in removing Cd^{2+} by varying the batch parameters in this study. The SEM images revealed significant changes in the surface structure of the LDH/F-bentonite composite after the bentonite was mixed with LDH (NiAl). The EDX analyses of the F-bentonite, LDH (NiAl), and the LDH/F-bentonite composite after adsorption of Cd^{2+} exhibited certain changes in their elemental weight percentages, confirming the adsorption of Cd^{2+} onto the surface of the studied adsorbents. The FTIR spectrograms of the studied adsorbents before and after adsorption showed some slight changes, indicating that surface hydroxyl groups were engaged in the adsorption process. The analysis also confirmed the successful loading of LDH (NiAl) onto F-bentonite and the adsorption of Cd^{2+} onto the F-bentonite, LDH (NiAl), and LDH/F-bentonite composite, suggesting ion-exchange and surface precipitation as the main controlling mechanisms for the formation of the adsorbent.

A retention time of 60 min was estimated to be the equilibrium contact time for the current adsorption system, with the LDH/F-bentonite composite presenting the highest adsorption capacity (60 mg g^{-1}) and removal efficiency (nearly 90% with a corresponding adsorption capacity of 22.5 mg g^{-1}) as compared with the other adsorbents at the respective retention times. With respect to the solution pH, an optimum performance at a pH value of 7.0 ± 0.2 was observed for all the adsorbents with little or insignificant changes with further increases in the solution pH. The LDH/F-bentonite composite adsorbent presented the highest removal efficiency and maximum adsorption capacity, while the LDH (NiAl) adsorbent showed the poorest performance as compared with the other adsorbents. The initial concentration of Cd^{2+} was also optimized for the best performance of the adsorption system for all the adsorbents, with the F-bentonite and LDH/F-bentonite adsorbents yielding the maximum adsorption capacity. A steady increase in the uptake capacity of Cd^{2+} was observed by increasing the dosage of the adsorbents, with the LDH/F-bentonite composite having the highest removal efficiency. The findings of the current study demonstrated the successful adsorption of Cd^{2+} onto the F-bentonite, LDH (NiAl), and LDH/F-bentonite composite, and suggest that the main controlling mechanisms of the formation of adsorbent are ion exchange and surface precipitation. The optimum performance of the composite adsorbent with respect to its adsorption capacity and removal efficiency indicate that the novel combination of the studied LDH and the functionalized bentonite clay can be used as an effective material for used in the removal of similar contaminants from wastewater systems in the future.

Author Contributions: Conceptualization, M.S. and M.T.A.; methodology, M.S.; software, A.A.A.; validation, M.S. and A.A.A.; formal analysis, M.S. and M.T.A.; investigation, M.S. and M.T.A.; resources, A.A.A.; data curation, M.S. and A.A.A.; writing—original draft preparation, M.S. and M.T.A.; writing—review and editing, M.S. and A.A.A.; visualization, A.A.A.; supervision, M.S. and M.T.A.; project administration, A.A.A. and M.T.A.; funding acquisition, M.T.A. All authors have read and agreed to the published version of the manuscript.

Funding: The authors extend their appreciation to the Deputyship for Research & Innovation, Ministry of Education in Saudi Arabia for funding this research work through the project no. (IFKSURG-2-894).

Conflicts of Interest: The authors declare no conflict of interest.

References

1. Celik, A.; Baker, D.R.; Arslan, Z.; Zhu, X.; Blanton, A.; Nie, J.; Yang, S.; Ma, S.; Han, F.X.; Islam, S.M. Highly Efficient, Rapid, and Concurrent Removal of Toxic Heavy Metals by the Novel 2D Hybrid LDH-[Sn₂S₆]. *Chem. Eng. J.* **2021**, *426*, 131696. [[CrossRef](#)]
2. Ritchie, H.; Roser, M. Clean Water and Sanitation. In *Our World in Data*; Oxford University Press: Oxford, UK, 2021.
3. Singh, D.; Gautam, R.K.; Kumar, R.; Shukla, B.K.; Shankar, V.; Krishna, V. Citric Acid Coated Magnetic Nanoparticles: Synthesis, Characterization and Application in Removal of Cd(II) Ions from Aqueous Solution. *J. Water Process Eng.* **2014**, *4*, 233–241. [[CrossRef](#)]
4. Wu, X.; Cobbina, S.J.; Mao, G.; Xu, H.; Zhang, Z.; Yang, L. A Review of Toxicity and Mechanisms of Individual and Mixtures of Heavy Metals in the Environment. *Environ. Sci. Pollut. Res. Int.* **2016**, *23*, 8244–8259. [[CrossRef](#)] [[PubMed](#)]

5. Ozverdi, A.; Erdem, M. Cu^{2+} , Cd^{2+} and Pb^{2+} Adsorption from Aqueous Solutions by Pyrite and Synthetic Iron Sulphide. *J. Hazard. Mater.* **2006**, *137*, 626–632. [[CrossRef](#)] [[PubMed](#)]
6. Tang, C.; Shu, Y.; Zhang, R.; Li, X.; Song, J.; Li, B.; Zhang, Y.; Ou, D. Comparison of the Removal and Adsorption Mechanisms of Cadmium and Lead from Aqueous Solution by Activated Carbons Prepared from Typha Angustifolia and Salix Matsudana. *RSC Adv.* **2017**, *7*, 16092–16103. [[CrossRef](#)]
7. Elbedwehy, A.M.; Abou-Elanwar, A.M.; Ezzat, A.O.; Atta, A.M. Super Effective Removal of Toxic Metals Water Pollutants Using Multi Functionalized Polyacrylonitrile and Arabic Gum Grafts. *Polymers* **2019**, *11*, 1938. [[CrossRef](#)]
8. Sarode, S.; Upadhyay, P.; Khosa, M.A.; Mak, T.; Shakir, A.; Song, S.; Ullah, A. Overview of Wastewater Treatment Methods with Special Focus on Biopolymer Chitin-Chitosan. *Int. J. Biol. Macromol.* **2019**, *121*, 1086–1100. [[CrossRef](#)]
9. Skoczko, I.; Szatylowicz, E. Removal of Heavy Metal Ions by Filtration on Activated Alumina-Assisted Magnetic Field. *Desalination Water Treat.* **2018**, *117*, 345–352. [[CrossRef](#)]
10. Elboughdiri, N. The Use of Natural Zeolite to Remove Heavy Metals Cu (II), Pb (II) and Cd (II), from Industrial Wastewater. *Cogent Eng.* **2020**, *7*, 1782623. [[CrossRef](#)]
11. Yang, J.; Hou, B.; Wang, J.; Tian, B.; Bi, J.; Wang, N.; Li, X.; Huang, X. Nanomaterials for the Removal of Heavy Metals from Wastewater. *Nanomaterials* **2019**, *9*, 424. [[CrossRef](#)]
12. Parvin, F.; Rikta, S.Y.; Tareq, S.M. 8—Application of Nanomaterials for the Removal of Heavy Metal from Wastewater. In *Nanotechnology in Water and Wastewater Treatment*; Ahsan, A., Ismail, A.F., Eds.; Micro and Nano Technologies; Elsevier: Amsterdam, The Netherlands, 2019; pp. 137–157, ISBN 978-0-12-813902-8.
13. Wang, Z.; Zhang, L.; Fang, P.; Wang, L.; Wang, W. Study on Simultaneous Removal of Dye and Heavy Metal Ions by NiAl-Layered Double Hydroxide Films. *ACS Omega* **2020**, *5*, 21805–21814. [[CrossRef](#)] [[PubMed](#)]
14. Gu, S.; Kang, X.; Wang, L.; Lichtfouse, E.; Wang, C. Clay Mineral Adsorbents for Heavy Metal Removal from Wastewater: A Review. *Environ. Chem. Lett.* **2019**, *17*, 629–654. [[CrossRef](#)]
15. He, W.; Ai, K.; Ren, X.; Wang, S.; Lu, L. Inorganic Layered Ion-Exchangers for Decontamination of Toxic Metal Ions in Aquatic Systems. *J. Mater. Chem. A* **2017**, *5*, 19593–19606. [[CrossRef](#)]
16. He, X.; Qiu, X.; Chen, J. Preparation of Fe(II)–Al Layered Double Hydroxides: Application to the Adsorption/Reduction of Chromium. *Colloids Surf. A Physicochem. Eng. Asp.* **2017**, *516*, 362–374. [[CrossRef](#)]
17. Puzyrnaya, L.; Pshinko, G.; Zub, V.; Zuy, O. Removal of Cu(II), Co(II) and Cd(II) from Water Solutions by Layered-Double Hydroxides with Different [Mg(II)]/[Fe(III)] Molar Ratios. *Bull. Mater. Sci.* **2020**, *43*, 3. [[CrossRef](#)]
18. Johnston, A.-L.; Lester, E.; Williams, O.; Gomes, R.L. Understanding Layered Double Hydroxide Properties as Sorbent Materials for Removing Organic Pollutants from Environmental Waters. *J. Environ. Chem. Eng.* **2021**, *9*, 105197. [[CrossRef](#)]
19. Li, Z.; Yang, B.; Zhang, S.; Wang, B.; Xue, B. A Novel Approach to Hierarchical Sphere-like ZnAl-Layered Double Hydroxides and Their Enhanced Adsorption Capability. *J. Mater. Chem. A* **2014**, *2*, 10202–10210. [[CrossRef](#)]
20. Moaty, S.A.A.; Farghali, A.; Moussa, M.; Khaled, R. Remediation of Waste Water by Co–Fe Layered Double Hydroxide and Its Catalytic Activity. *J. Taiwan Inst. Chem. Eng.* **2017**, *71*, 441–453. [[CrossRef](#)]
21. Rojas, R. Copper, Lead and Cadmium Removal by Ca Al Layered Double Hydroxides. *Appl. Clay Sci.* **2014**, *87*, 254–259. [[CrossRef](#)]
22. Kundu, S.; Naskar, M.K. Carbon-Layered Double Hydroxide Nanocomposite for Efficient Removal of Inorganic and Organic Based Water Contaminants—Unravelling the Adsorption Mechanism. *Mater. Adv.* **2021**, *2*, 3600–3612. [[CrossRef](#)]
23. Liao, W.; Wang, H.; Li, H.; Yang, P. Cd(II) Removal by Fe(II) Surface Chemically Modified Layered Double Hydroxide–Graphene Oxide: Performance and Mechanism. *RSC Adv.* **2019**, *9*, 38982–38989. [[CrossRef](#)] [[PubMed](#)]
24. Gu, Z.; Atherton, J.J.; Xu, Z.P. Hierarchical Layered Double Hydroxide Nanocomposites: Structure, Synthesis and Applications. *Chem. Commun.* **2015**, *51*, 3024–3036. [[CrossRef](#)] [[PubMed](#)]
25. Shan, R.; Yan, L.; Yang, K.; Yu, S.; Hao, Y.; Yu, H.; Du, B. Magnetic Fe₃O₄/MgAl-LDH Composite for Effective Removal of Three Red Dyes from Aqueous Solution. *Chem. Eng. J.* **2014**, *252*, 38–46. [[CrossRef](#)]
26. Daud, M.; Kamal, M.S.; Shehzad, F.; Al-Harathi, M.A. Graphene/Layered Double Hydroxides Nanocomposites: A Review of Recent Progress in Synthesis and Applications. *Carbon* **2016**, *104*, 241–252. [[CrossRef](#)]
27. Hussain, S.T.; Ali, S.A.K. Removal of Heavy Metal by Ion Exchange Using Bentonite Clay. *J. Ecol. Eng.* **2021**, *22*, 104–111. [[CrossRef](#)]
28. Bulut, E.; Özacar, M.; Şengil, İ.A. Equilibrium and Kinetic Data and Process Design for Adsorption of Congo Red onto Bentonite. *J. Hazard. Mater.* **2008**, *154*, 613–622. [[CrossRef](#)]
29. Wang, C.-C.; Juang, L.-C.; Hsu, T.-C.; Lee, C.-K.; Lee, J.-F.; Huang, F.-C. Adsorption of Basic Dyes onto Montmorillonite. *J. Colloid Interface Sci.* **2004**, *273*, 80–86. [[CrossRef](#)]
30. Jia, Y.; Zhang, Y.; Fu, J.; Yuan, L.; Li, Z.; Liu, C.; Zhao, D.; Wang, X. A Novel Magnetic Biochar/MgFe-Layered Double Hydroxides Composite Removing Pb^{2+} from Aqueous Solution: Isotherms, Kinetics and Thermodynamics. *Colloids Surf. A Physicochem. Eng. Asp.* **2019**, *567*, 278–287. [[CrossRef](#)]
31. Yu, J.; Zhu, Z.; Zhang, H.; Qiu, Y.; Yin, D. Mg–Fe Layered Double Hydroxide Assembled on Biochar Derived from Rice Husk Ash: Facile Synthesis and Application in Efficient Removal of Heavy Metals. *Environ. Sci. Pollut. Res.* **2018**, *25*, 24293–24304. [[CrossRef](#)]
32. Zhou, H.; Jiang, Z.; Wei, S.; Liang, J. Adsorption of Cd(II) from Aqueous Solutions by a Novel Layered Double Hydroxide FeMnMg-LDH. *Water Air Soil Pollut.* **2018**, *229*, 78. [[CrossRef](#)]

33. Ma, L.; Wang, Q.; Islam, S.M.; Liu, Y.; Ma, S.; Kanatzidis, M.G. Highly Selective and Efficient Removal of Heavy Metals by Layered Double Hydroxide Intercalated with the MoS_4^{2-} Ion. *J. Am. Chem. Soc.* **2016**, *138*, 2858–2866. [[CrossRef](#)] [[PubMed](#)]
34. Wang, S.-L.; Wang, P.-C. In Situ XRD and ATR-FTIR Study on the Molecular Orientation of Interlayer Nitrate in Mg/Al-Layered Double Hydroxides in Water. *Colloids Surf. A Physicochem. Eng. Asp.* **2007**, *292*, 131–138. [[CrossRef](#)]
35. Guan, X.; Yuan, X.; Zhao, Y.; Bai, J.; Li, Y.; Cao, Y.; Chen, Y.; Xiong, T. Adsorption Behaviors and Mechanisms of Fe/Mg Layered Double Hydroxide Loaded on Bentonite on Cd (II) and Pb (II) Removal. *J. Colloid Interface Sci.* **2022**, *612*, 572–583. [[CrossRef](#)] [[PubMed](#)]
36. Wang, S.; Dong, Y.; He, M.; Chen, L.; Yu, X. Characterization of GMZ Bentonite and Its Application in the Adsorption of Pb(II) from Aqueous Solutions. *Appl. Clay Sci.* **2009**, *43*, 164–171. [[CrossRef](#)]
37. Guo, Y.; Zhu, Z.; Qiu, Y.; Zhao, J. Adsorption of Arsenate on Cu/Mg/Fe/La Layered Double Hydroxide from Aqueous Solutions. *J. Hazard. Mater.* **2012**, *239–240*, 279–288. [[CrossRef](#)]
38. Tang, H.; Zhou, W.; Zhang, L. Adsorption Isotherms and Kinetics Studies of Malachite Green on Chitin Hydrogels. *J. Hazard. Mater.* **2012**, *209–210*, 218–225. [[CrossRef](#)]
39. Chowdhury, S.; Mishra, R.; Saha, P.; Kushwaha, P. Adsorption Thermodynamics, Kinetics and Isothermic Heat of Adsorption of Malachite Green onto Chemically Modified Rice Husk. *Desalination* **2011**, *265*, 159–168. [[CrossRef](#)]
40. Taty-Costodes, V.C.; Fauduet, H.; Porte, C.; Delacroix, A. Removal of Cd(II) and Pb(II) Ions, from Aqueous Solutions, by Adsorption onto Sawdust of Pinus Sylvestris. *J. Hazard. Mater.* **2003**, *105*, 121–142. [[CrossRef](#)]
41. Karapinar, N.; Donat, R. Adsorption Behaviour of Cu^{2+} and Cd^{2+} onto Natural Bentonite. *Desalination* **2009**, *249*, 123–129. [[CrossRef](#)]
42. Raji, F.; Pakizeh, M. Study of Hg(II) Species Removal from Aqueous Solution Using Hybrid ZnCl₂-MCM-41 Adsorbent. *Appl. Surf. Sci.* **2013**, *282*, 415–424. [[CrossRef](#)]
43. Hameed, B.H.; El-Khaiary, M.I. Batch Removal of Malachite Green from Aqueous Solutions by Adsorption on Oil Palm Trunk Fibre: Equilibrium Isotherms and Kinetic Studies. *J. Hazard. Mater.* **2008**, *154*, 237–244. [[CrossRef](#)] [[PubMed](#)]
44. Ayranci, E.; Duman, O. Structural Effects on the Interactions of Benzene and Naphthalene Sulfonates with Activated Carbon Cloth during Adsorption from Aqueous Solutions. *Chem. Eng. J.* **2010**, *156*, 70–76. [[CrossRef](#)]
45. Duman, O.; Özcan, C.; Gürkan Polat, T.; Tunç, S. Carbon Nanotube-Based Magnetic and Non-Magnetic Adsorbents for the High-Efficiency Removal of Diquat Dibromide Herbicide from Water: OMWCNT, OMWCNT-Fe₃O₄ and OMWCNT- κ -Carrageenan-Fe₃O₄ Nanocomposites. *Environ. Pollut.* **2019**, *244*, 723–732. [[CrossRef](#)] [[PubMed](#)]
46. Malik, P.K. Use of Activated Carbons Prepared from Sawdust and Rice-Husk for Adsorption of Acid Dyes: A Case Study of Acid Yellow 36. *Dye. Pigment.* **2003**, *56*, 239–249. [[CrossRef](#)]
47. Kumar, P.S.; Ramakrishnan, K.; Gayathri, R. Removal of Nickel(II) from Aqueous Solutions by Ceralite IR 120 Cationic Exchange Resins. *J. Eng. Sci. Technol.* **2010**, *5*, 232–243.
48. Muralisankar, I.; Agilan, S.; Selvakumar, R.; Vairam, S. Synthesis of Co₃O₄/graphene nanocomposite using paraffin wax for adsorption of methyl violet in water. *IET Nanobiotechnology* **2018**, *12*, 787–794. [[CrossRef](#)]
49. Aljamali, N.M.; Khdur, R.A.; Alfatlawi, I.O. Physical and chemical adsorption and its applications. *Int. J. Thermodyn. Chem. Kinet.* **2021**, *7*, 1–8. [[CrossRef](#)]
50. Tchanang, G.; Djangang, C.N.; Abi, C.F.; Moukouri, D.L.M.; Djabo, G.T.N.; Kepdieu, J.M.; Blanchart, P. Nano-silica from kaolinitic clay used as adsorbent for anionic and cationic dyes removal: Linear and non-linear regression isotherms and kinetics studies. *Ann. Civ. Environ. Eng.* **2022**, *6*, 8–18. [[CrossRef](#)]
51. Gimbert, F.; Morin-Crini, N.; Renault, F.; Badot, P.-M.; Crini, G. Adsorption Isotherm Models for Dye Removal by Cationized Starch-Based Material in a Single Component System: Error Analysis. *J. Hazard. Mater.* **2008**, *157*, 34–46. [[CrossRef](#)]
52. Abtahi, M.; Mesdaghinia, A.; Saeedi, R.; Nazmara, S. Biosorption of As(III) and As(V) from Aqueous Solutions by Brown Macroalga Colpomenia Sinuosa Biomass: Kinetic and Equilibrium Studies. *Desalination Water Treat.* **2013**, *51*, 3224–3232. [[CrossRef](#)]
53. Naddafi, K.; Rastkari, N.; Nabizadeh, R.; Saeedi, R.; Gholami, M.; Sarkhosh, M. Adsorption of 2,4,6-Trichlorophenol from Aqueous Solutions by a Surfactant-Modified Zeolitic Tuff: Batch and Continuous Studies. *Desalination Water Treat.* **2016**, *57*, 5789–5799. [[CrossRef](#)]
54. Günay, A.; Arslankaya, E.; Tosun, İ. Lead Removal from Aqueous Solution by Natural and Pretreated Clinoptilolite: Adsorption Equilibrium and Kinetics. *J. Hazard. Mater.* **2007**, *146*, 362–371. [[CrossRef](#)] [[PubMed](#)]